Contents lists available at ScienceDirect

# Nuclear Instruments and Methods in Physics Research B

journal homepage: www.elsevier.com/locate/nimb



# Comparison of proton and helium induced M subshell X-ray production cross sections with the ECUSAR theory



D.D. Cohen a,\*, E. Stelcer , J. Crawford , A. Atanacio , G. Doherty , G. Lapicki b

- <sup>a</sup> Australian Nuclear Science and Technology Organisation, Locked Bag 2001, Kirrawee DC, NSW 2232, Australia
- <sup>b</sup> Department of Physics, East Carolina University, Greenville, NC 27858, USA

#### ARTICLE INFO

Article history: Received 18 February 2013 Received in revised form 29 April 2013 Accepted 27 May 2013 Available online 19 July 2013

Keywords: Protons He ions X-rays PIXE M-subshell **ECUSAR** 

#### ABSTRACT

M subshell X-ray production cross sections have been measured for  $M\alpha_{12}$ ,  $M\beta_1$ ,  $M\gamma$ ,  $M_2-N_4$  and  $M_1-O_{23}$ transitions representing all five M subshells. These experimental cross sections have been compared with the ECUSAR theory of Lapicki and four parameter fits are given to the experiment to theory ratios covering the proton and helium ion energy range from 0.5 to 3 MeV on thin W, Au, Pb, Th and U targets.

© 2013 Elsevier B.V. All rights reserved.

### 1. Introduction

Particle induced X-ray emission (PIXE) has been used by many laboratories for many years to characterise a broad range of samples. Current PIXE detection systems are readily capable of measuring X-rays between 1 and 20 keV and hence through the characteristic X-rays from K and L shells cover most elements in the periodic table for aluminium upwards. For common heavy elements with characteristic X-rays in the 1-5 keV region it has become more important to better understand and theoretically predict the numerous M shell lines which often overlap with lighter element K and L shell lines. M shell ionisation cross sections have been measured for more than a quarter of a century [1]. More recently the focus has shifted to more accurate measurements of the five M subshell X-ray production cross sections [2–8] to better quantify these and to make comparisons with theory across all five

The ECPSSR theory developed over the years by Brandt and Lapicki [9] and applied specifically to the M shell [10], has more recently been extended to the ECUSAR theory [11]. Here the experimental and the ECUSAR X-ray production cross sections are compared for dominant lines in each of the five M subshells for slow proton and helium ion impact on selected high atomic number targets from W to U. This covers the X-ray energy range 1.1-5.5 keV.

Proton energies between 0.5 and 3 MeV and helium ion energies between 0.5 and 2 MeV were used to provide M subshell cross sections for 0.3 <  $\xi_{_{\rm Mi}}$  < 3, where the reduced velocity  $\xi_{_{\rm Mi}}$  = 2 $v_1/(\theta_{_{\rm Mi}}v_{_2{\rm Mi}})$ , was defined by Brandt and Lapicki [12] and distinguishes between the slow ( $\xi_{Mi}$  < 1) and the fast ( $\xi_{Mi}$  > 1) collision regimes.

#### 2. Experimental conditions

Five Mylar foils with thin metal coatings evaporated on their front surfaces were used as targets. Table 1 gives the metal film characteristics including typical detector efficiencies and self absorption for the corresponding M line energies. Target thicknesses were calibrated to ±5% by standard Rutherford backscattering (RBS) techniques. Self-absorption corrections for these thin targets were generally less than 6% and ion energy losses for the lowest proton and helium ion energies (0.5 MeV) were less 5 and 19 keV, respectively.

Each target was bombarded with 10-20 nA of beam current for between 20 and 60 µC of ion charge. This was sufficient to keep counting statistical errors for each major M subshell peak below 10%. A modern VORTEX X-ray detector was used with a 25 µm beryllium window and a 400 µm thick silicon chip.

## 3. Results

Fig. 1 shows a theoretical M shell PIXE spectrum without the background for 3 MeV protons on U. It was generated in the

<sup>\*</sup> Corresponding author. E-mail address: dcz@ansto.gov.au (D.D. Cohen).

**Table 1**Thin target characteristics used for this study.

Target	Thickness (μg/cm²) ±5%	Detector efficiency for $M\alpha$ line	Self absorption for $M\alpha$ line	$\Delta E$ (keV) for 0.5 MeV protons	$\Delta E$ (keV) for 0.5 MeV helium	Range of energies for M lines (keV)
WO <sub>3</sub>	48.1	0.231	0.939	3.30	14.3	1.1-2.9
Au	46.6	0.420	0.977	4.01	15.8	1.4-3.6
Pb	49.6	0.522	0.977	4.44	18.8	1.6-3.9
$ThF_4$	45.8	0.728	0.977	3.18	14.3	2.1-5.2
$UF_4$	45.3	0.763	0.977	2.96	14.1	2.2-5.5

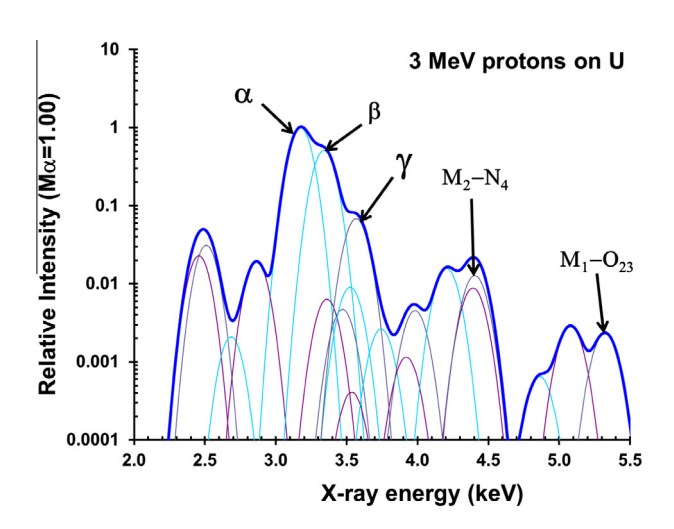
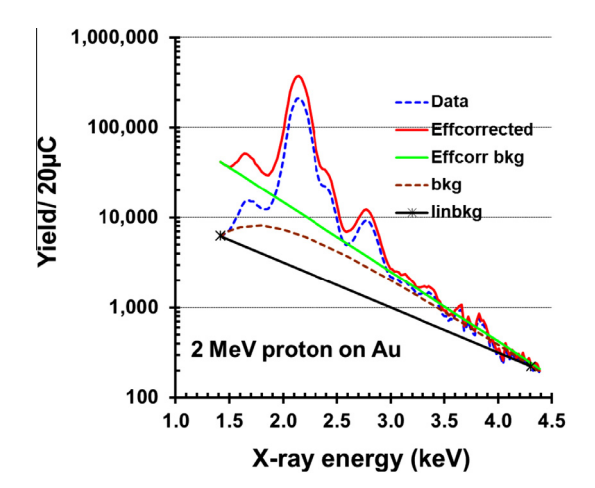


Fig. 1. Theoretical M shell spectrum (no background) normalised to the  $M\alpha$  peak with 22 Gaussian M line transitions for 3 MeV protons on thin U.

**Table 2**Key M line transitions associated with individual M subshells and their possible overlap transitions used for our targets W–U.

_				
	Sub-shell	Major line	Transition	Overlaps not fitted
	M <sub>5</sub>	$M\alpha_{12}$	M <sub>5</sub> -N <sub>67</sub>	$M_3$ - $N_1$
	$M_4$	$M\beta_1$	$M_4 - N_6$	$M_5-O_3$ , $M_4-O_{23}$
	$M_3$	Μγ	$M_3 - N_5$	$M_3-N_4$ , $M_2-N_1$ , $M_3-O_1$
	$M_2$	$Mm_1$	$M_2-N_4$	$M_1-N_{23}$ , $M_3-O_1$ , $M_3-O_{67}$
	$M_1$		$M_1-O_{23}$	$M_2$ - $O_1$



**Fig. 2.** Typical background subtraction technique for 2 MeV protons on a thin Au foil [13]. The dashed curves are original data, the solid curves are the efficiency corrected data described in the text.

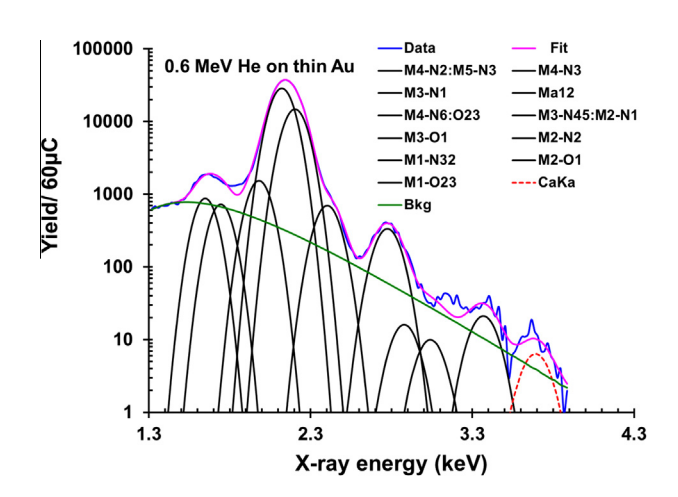


**Fig. 3.** Fit of 11 Gaussians M line transitions (solid lines) and the CaK $\alpha$  line (dashed line) to 0.6 MeV helium ion spectrum (with background) on a thin Au target.

standard way [13] by generating 22 Gaussians at fixed known energies, representing 22 M line transitions, with these Gaussians having variable experimental X-ray detector resolutions (between 120 eV at 2 keV and 180 eV at 6 keV) and detector efficiencies the same as the experimental efficiencies used in the present work.

The relative intensities were calculated using the ECUSAR subshell ionisation cross sections [11], the DHS fluorescence yields and emission rates of Puri [14] and the Coster–Kronig rates of Chauhan and Puri [15].

These 22 M lines varied in intensity over four orders of magnitude and a plot of this type was used to identify both individual Gaussians to fit to the experimental data as well as any possible key overlaps not fitted by separate Gaussians. There was no need to use Gaussians with low energy tails as the response function for our detector had low energy tail contributions to the total peak area well below 1% for all lines considered here. Table 2 shows the overlaps (not fitted separately) for the major lines used in the current work to represent each of the five M subshells. The main problematic line was the  $(M_2-N_1)$  shown in Fig. 1 which can for some elements have  $(M_1-N_{23})$  line interferences. We overcome this by adding the theoretical ECUSAR  $(M_2-N_1)$  and  $(M_1-N_{23})$  contributions together for comparison with the experiment for this line.

Appropriate background subtraction under the characteristic M lines for experimental spectra was critical, especially for the low intensity lines. Fig. 2 demonstrates the background subtraction method used here and described in detail in Ref. [13]. Basically, the experimental spectrum (dashed curve in Fig. 2) was divided by the detector efficiency in the range 1.1–5.5 keV and a linear background on a log-linear plot fitted and subtracted from it (solid curve in Fig. 2). The background obtained in this way (dashed curve under the data of Fig. 2) is compared with a standard linear background (solid line with \*) in the same figure. This background removedspectrum was then recorrected for detector efficiency and the relevant M shell Gaussians fitted to obtain peak areas for

## Download English Version:

# https://daneshyari.com/en/article/1681693

Download Persian Version:

https://daneshyari.com/article/1681693

<u>Daneshyari.com</u>